Lasers in Manufacturing Conference 2019

Measurement of thermal cycle at multi-pass layer build-up with different travel path strategies during DLMD process

Stanislav Stankevich[a], Andrey Gumenyuk [b*], Anne Strasse [b], Michael Rethmeier [b,c]

[a]*St.Petersburg Polytechnic University, St. Petersburg, Russia*
[b]*Bundesanstalt für Materialforschung und -prüfung (BAM), Berlin, Germany*
[c]*Technische Universität Berlin, Germany*

Abstract

The shape of the parts, created by the technology of direct laser metal deposition (DLMD), is influenced by various parameters, for example, the power and diameter of the laser source spot. The contribution of energy from the laser affects the temperature distribution in the formed layers. The changing temperature in the working area entails a change in the geometry of the layers and affects the stability of the process. In this paper, experiments on the measurement of temperature cycles in the DLMD process with different directions of the filling track are carried out. An infrared camera was used to measure thermal cycles. The calibration of the acquired data (i.e. correspondence table between the intensity of thermal radiation of the material and the absolute temperature) was done with help of two-color pyrometer ex situ and in situ measurements. The experiments are carried out on two materials 316L and Inconel 718. The effect of the maximum temperature on the layer height is shown, and thermal cycles in the formation of layers for different filling strategies are presented.

Keywords: additive technology; laser metal deposition; thermal cycles; stainless steel 316L

1. Introduction

Nowadays additive manufacturing (AM) has taken its place in materials processing technologies. AM technologies permit companies a fast and cost-effective improvement process. The most progressive

* Corresponding author. Tel.: +49 3081044623;
E-mail address: Andrey.gumenyuk@bam.de.

additive technology is DLMD because it has a high production capacity and the ability to create large scale products for the aviation and aerospace industry Vildanov et al. 2016. The method of DLMD is a complex multifactorial process which influenced by various parameters Klimova-Korsmik et al. 2016. The search for the technological mode, taking into account all the features of the additive machine Turichin et al. 2016 and maintaining the stability of the process in the manufacture of the product is not a trivial task Turichin et.al 2016.

One of important factors in the stability of the DLMD process is the temperature distribution in both the deposited portion of the sample and the heat sink of the substrate, as well as temperature cycles applied to the material. In DLMD process, stable layer growth and constant melt pool temperature indicates both good geometrical accuracy Song et al. 2012 and metallurgical property Peyre at al. 2008. Usually, pyrometers Doubensaia et al. 2004 and thermocouples have been employed to monitor the melt pool temperature Petrat et al 2017. Among these sensors, thermo cameras provide the most comprehensive information about the process with limited processing speed caused by demanding image processing. The task of the study of temperature cycles in the DLMD process is relevant and was carried out by many authors Everton et al. 2016. Each of the previously used research methods has its strengths and weaknesses. Weaknesses include the many sensors used and their complex interaction and accuracy redundancy obtained with their help. As strengths, it is worth noting the good adaptability of the system for measuring temperature cycles in the material.

The experiments were performed to determine thermal cycles in the process of build-up from layer to layer, the effect of temperature cycles on the geometry of the layers and the stability of the process. A distinctive feature of the method which described in this article is a small amount of devices for making measurements and easy interpretation of the obtained data.

2. Experimental setup

In course of the work, an infrared camera NIT TACHYON 16k and a two-color pyrometer SENSORTHERM MQ22 have been used to measure the intensity of the thermal radiation of the build-up sample and for direct measurement of absolute temperature respectively. The technical characteristics of the devices are presented in tables 1 and 2, respectively.

The experiment consisted of two stages: 1) calibration of the MWIR-camera data i.e. construction of the correspondence table between the data of thermal radiation intensity recorded by the infrared camera and the pyrometer values; 2) capture of DLMD process by the infrared camera and analysis of the results.

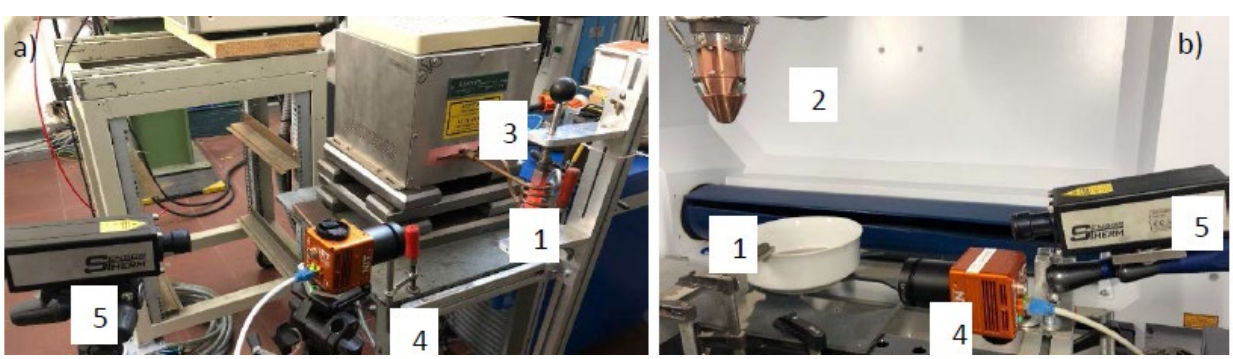

Fig. 1. Experimental setup a) calibration experiments b) build-up trials 1-specimen, 2 -DMD-nozzle; 3 -inductor; 4 -MWIR-camera; 5 -two-color pyrometer

In the first stage of the experiment, a sample of 316L steel (Fig. 1b) has been heated in an induction heater and after attaining of the temperature of around 1200 °C air cooled. The temperatures were registered by means of both an infrared camera and a pyrometer (Fig. 1a), The field of view of the infrared camera corresponded to 50 mm x 50 mm (see Fig.2 a) at resolution of 128 by 128 pixel and a measurements spot size diameter of the pyrometer was about 1 mm.

The second stage of the experiment was carried out using an infrared camera on the Trumf TruLaser Cell 3000 machine, which combines of a disk laser with a wavelength of 1,03 µm, a vibrating powder feeder Medicoat Flowmotion. The IR camera was captured thermal radiation during build-up of the sample. Helium was used as a transporting gas.

Table 1. Specifications of NIT TACHYON 16K infrared camera

NIT TACHYON 16k	
Detector type	VPD PbSe FPA with digital interface
Array format	128x128 pixels
Spectral range	MWIR, 1.0 to 5.0 [µm]
Peak wavelength of detection:	3.7 [µm]
Frame rate	50-2000 [fps]

Table 2. Specifications of the SENSORTHERM MQ22pyrometer

SENSORTHERM MQ22	
Measuring range	500-2000 [°C]
Emissivity ratio ε1/ε2	0.8 to 1.2
Emissivity ε (per channel)	0.05 to 1.2
Measurement uncertainty (T_{Amb} = 23[°C], t 90 = 1[s])	T < 1500[°C]: 0.3% of measured value in [°C] + 1[°C] T < 2500[°C]: 0.5% of measured value in [°C]+ 1[°C]
Repeatability (T_{Amb} = 23[°C], t 90 = 1[s]	0.1% of measured value in [°C] +1[°C]

3. Experimental setup

3.1. Calibration of MWIR-camera

In order to establish the correspondence table between the intensity of thermal radiation of the material and the absolute temperature, the heating and cooling cycle of the sample have been recorded by means of both measuring instruments. The data of the infrared camera have been averaged over a ROI marked as a red rectangle in Fig. 2a) and were compared with the data of the pyrometer. The maximum intensity or temperature was considered as the reference point. The temperature was measured in the range from 500 to 1200 °C. The intensity and temperature values were compared with the same time step from the initial point both for heating and cooling part of the thermal cycle. The experiment was carried out on samples of 316L steel and nickel-based alloy with two different signal amplification factors of the IR camera. To check the repeatability of the results of matching the intensity of thermal radiation and temperature, the heating and cooling cycle was repeated 5 times for each material and each mode of signal amplification of the IR camera. Fig. 2b shows groups of correspondence curves between the values of the average intensities measured by IR camera and absolute temperature values constructed on the basis of experimental data and being subject to linear extrapolation. The groups of the curves 1 and 2 correspond to nickel-based alloy at gain 1.25 and 1.5 respectively, and the groups of curves 3 and 4 to steel 316L for the same gain, respectively. As can be seen from the figure, the curves within a separate group are arranged heap and have no

significant deviations. In this regard, the resulting ratios between radiation intensities and absolute temperatures were taken as the group average for the material and the gain mode.

It should be noted that the state of the surface of the samples, i.e. the presence of scale or oxides, significantly affects the intensity of the thermal glow. This is clearly demonstrated by the experiment with heating and subsequent cooling of the fresh sample (Fig. 3a). The graph shows the temperature dependence on the intensity. The red line represents the heating of the new sample, at the top of the curve a scale was formed on the surface, after which the sample cooled in the air (blue line). For these reasons for the following experiments with nickel-based alloy a calibration routine has been made immediately during build up experiments by simultaneous measurement of temperature with MWIR camera and two-color pyrometer for a certain point at the specimen surface (see Fig. 1b).

3.2. Measurement of temperature cycles

During the experiment, a three-dimensional rectangular block with dimensions of 150x50x45 mm was deposited from 316L steel powder on a substrate of the same material. In the process of build-up, longitudinal and transverse filling strategies with sequential variation with the following technological parameters were used: laser radiation power P=1.2 kW, a linear velocity of the technological head V=1.3 m / min, spot diameter on the substrate d=2.4 mm and powder feeding rate m=17 g / min. The IR camera was located opposite the long wall at a distance of 300 mm. The camera FOV area was 47x47 mm. An example of the image obtained during the experiment is shown in Fig. 3b. The experiment was aborted on 50 layers as the process became unstable.

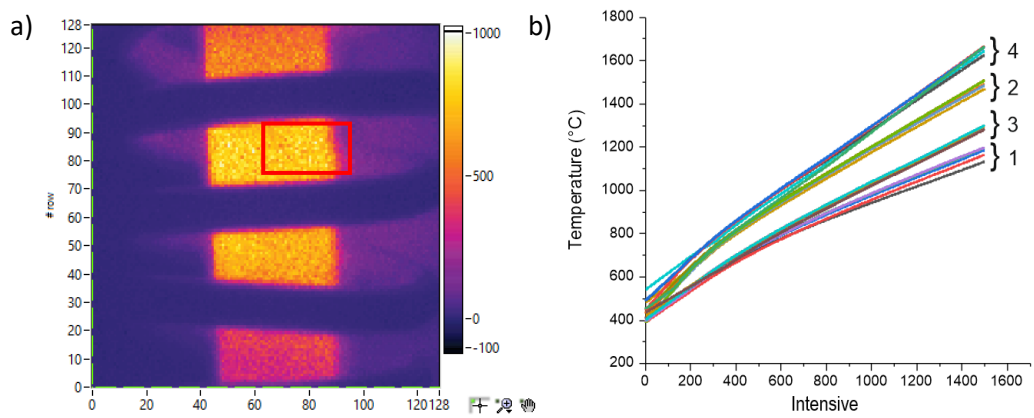

Fig. 2. a) The image obtained from the infrared camera; b) The curve of the temperature dependence on the intensity

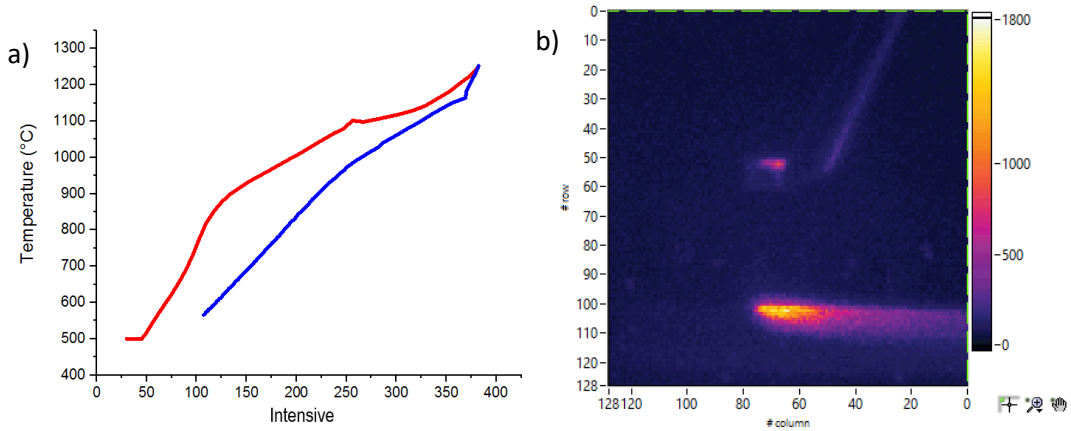

Fig. 3. a) Temperature dependence on intensity; red line-heating, blue line-cooling; b) The image obtained from the IR camera during the experiment

3.3. Analysis of experimental results

On the basis of the results obtained during the block build-up experiment, thermal cycles were constructed for the points located on the surface of the sample. The scheme of the location of the considered points is shown in Fig. 4. The positions of the points were analyzed relative to the lower right corner of the sample with

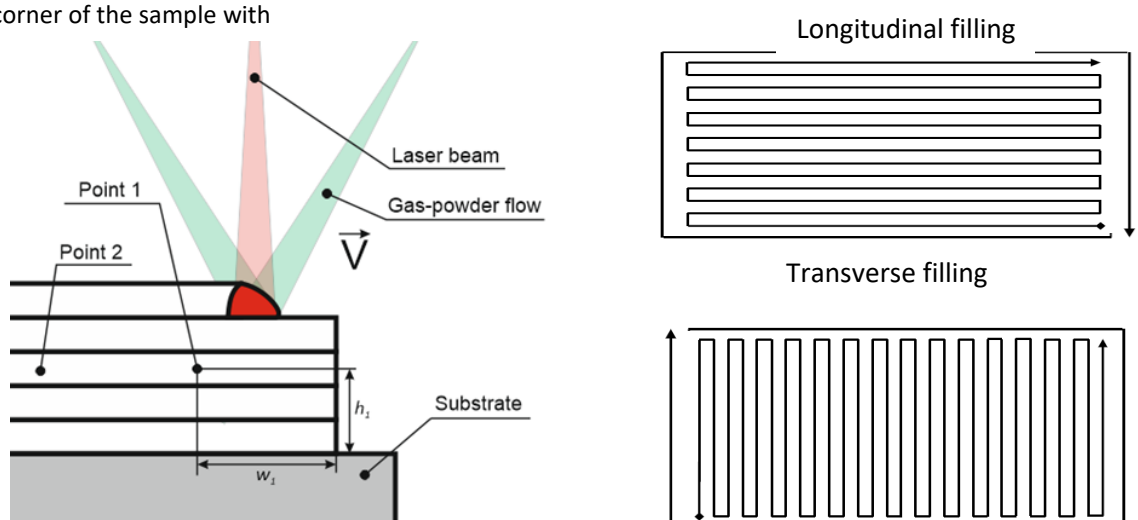

Fig. 4. Process scheme, build up strategies for odd and even layers

the corresponding horizontal w_n and vertical h_n components, where n is the point number. The horizontal component for the first point in the layer was assumed to be 5 mm (close to the edge), and for the second 45 mm (close to the middle). The vertical component of the points under consideration depends on the number of the correspondent layer and is determined by the height of the applied layer relative to the substrate.

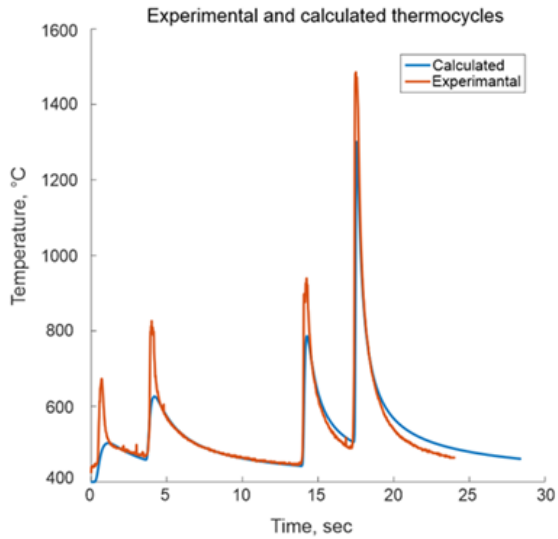

Fig. 5. Graph of the calculated and experimental thermal cycles for the longitudinal filling strategy

Thus, the thermal cycle displays the temperature changes in progress of the layer build-up and its subsequent heating when applying next layers. The experimental data were used for indirect verification of the analytical model described in Stankevich et al. 2018. With help of the model it is possible to set an arbitrary trajectory of the heat source. The calculated and experimental curves of the thermal cycle for the longitudinal filling strategy are presented in Fig. 5. As can be seen from the figure, the calculated curve has deviations in the places of temperature peaks. In the area of temperature decline, there is a fairly good coincidence of agreement between the curves. This can be explained, on the one hand, by a significant deviation in the values of thermal properties, the absorption coefficient of laser radiation and other properties of the material from the weighted average values at high temperatures. On the other hand, in the massive samples used in the experiment, the heat exchange with the environment is not as intensive as supposed by the model.

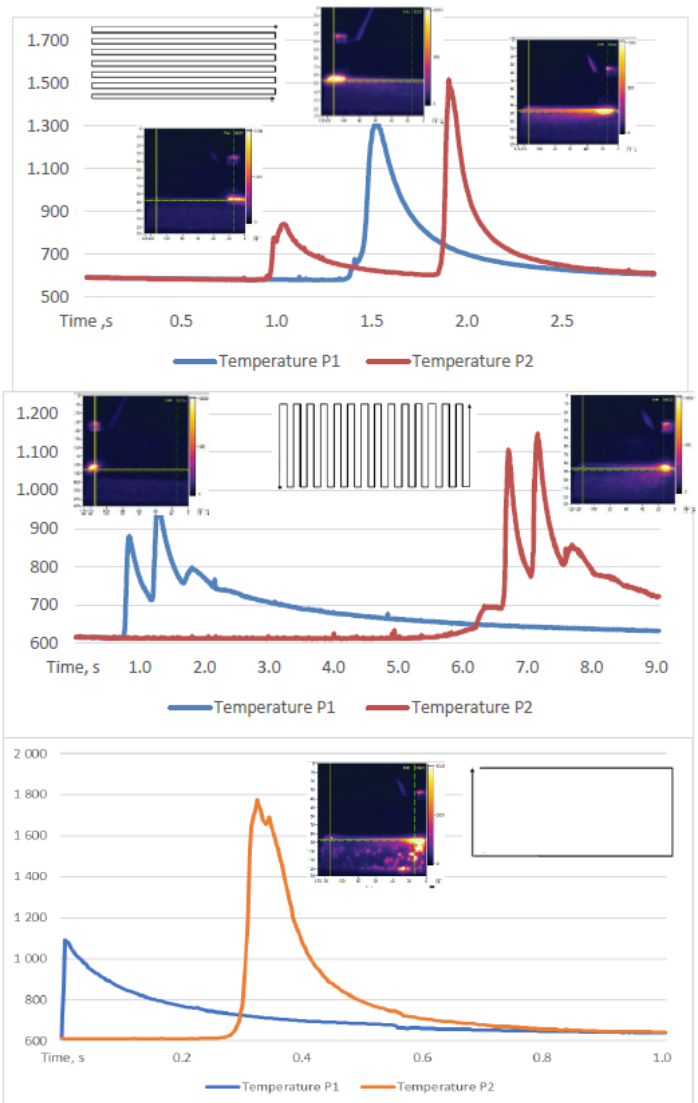

Fig. 6. Thermal cycles for 22nd and 23rd layers

Fig. 6 shows the thermal cycles for 22nd and 23rd layers, which correspond approximately to 16 mm a height above substrate plate level as well as snapshots of temperature distribution at different moment corresponding to peak temperature at control points P1 and P2. As can be seen from the thermal cycles, the point located closer to the center of the sample has normally a higher maximum temperature than the point near the edge, regardless of the layer and strategy. The transversal strategy results in smaller temperatures at the measuring points in compare to the longitudinal strategy. The last diagram represent the thermal cycle measured between layers 22 and 23 upon finishing contour track on the side directed to the IR camera´. A it can be seen, the measured temperature here is the highest and the temperature distribution plot reveals massive heating of the material on the side wall under the deposited layer.

It should be noted that the layer filling strategy affects the temperature gradient. For the longitudinal filling strategy, the temperature gradient is higher than for the transverse filling strategy. This is due to the effect of heating when applying for adjacent passes. In the case of a longitudinal filling strategy, the length of the applied passes is higher than the transverse filling strategy and the material has time to cool down. This affects the temperature gradient and cooling rate. Fig. 7 shows the temperature distribution in the direction of the longer side of the layer for the longitudinal and transverse filling strategy, as well as temperature gradients. Fig. 8 is similar to Fig. 7, but the distribution and gradients are in vertically downwards direction (i.e. from the point of the laser spot to the substrate).

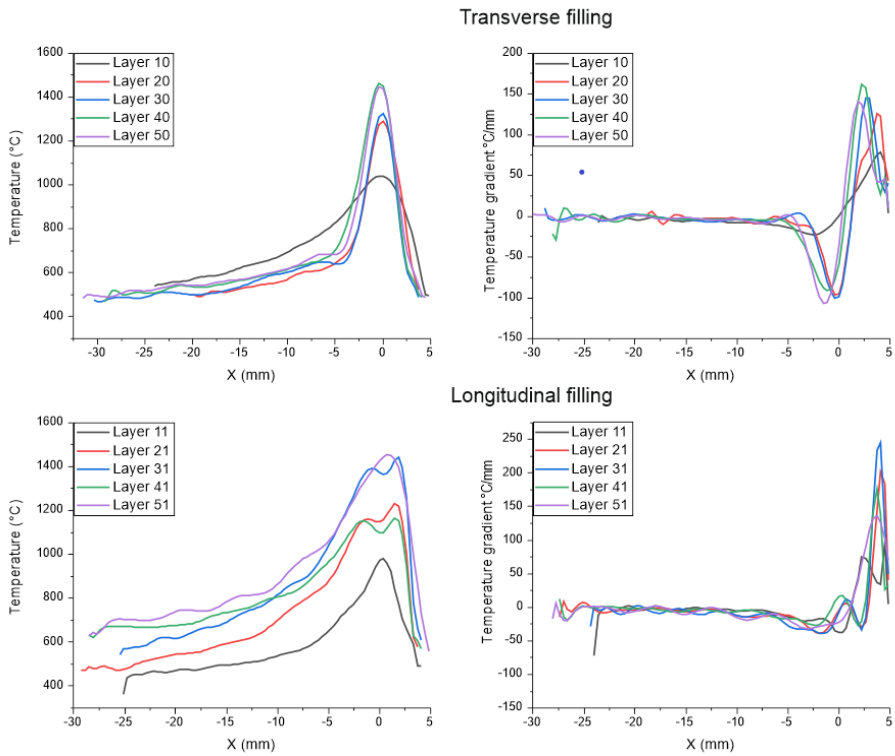

Fig. 7. Temperature distribution and temperature gradients in the direction of the longer side of the layer

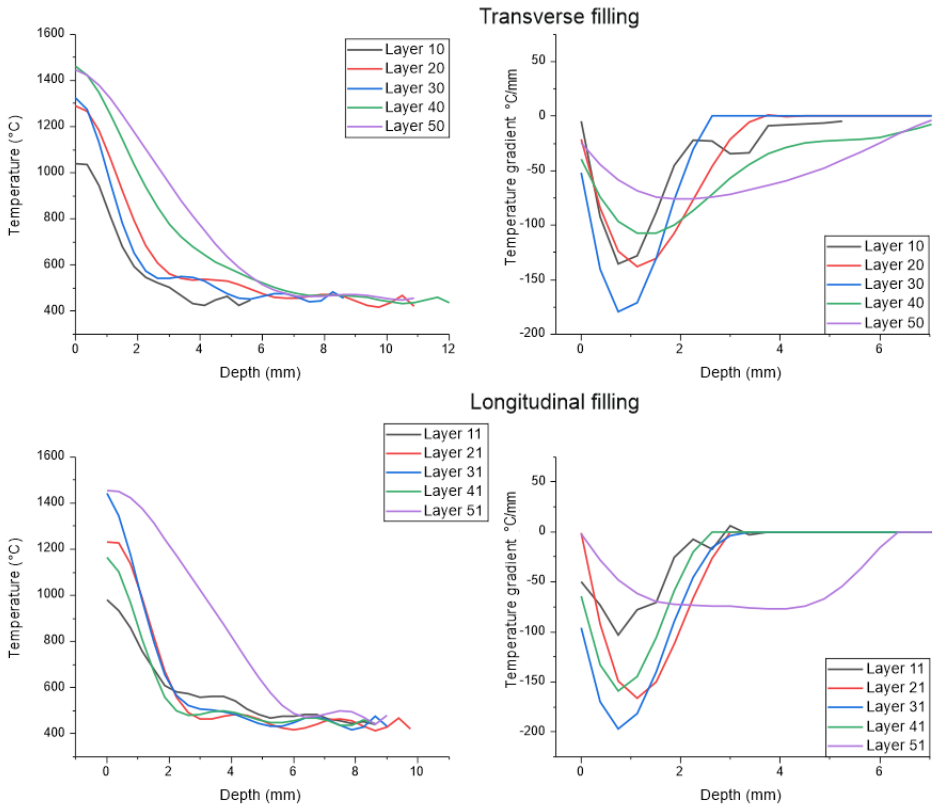

Fig. 8. Temperature distribution and temperature gradients in the direction from the point of exposure of the laser radiation towards the substrate for different layers

In the process of forming the sample its height was measured after each applied layer, as well as the maximum temperature in the area under consideration was captured by the IR camera. These data are presented in Fig. 9a. As can be seen from the graph there is a tendency of increasing the maximum temperature from layer to layer, while the layer height decreases.

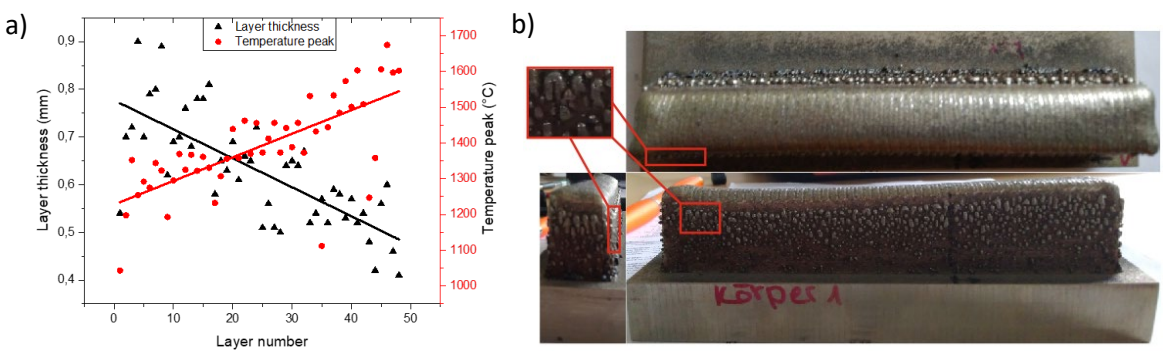

Fig. 9. a) Graphs of the maximum temperature in the melt pool area and layer height; b) Photo of the sample

Fig. 9b shows a photo of the sample, where multiple surface defects in the form of an upset metal as well as the deviation of the resulting shape are clearly visible. It should also be noted that the active formation of the upset metal began after 16 layers. It can be assumed that the occurrence of defects is associated with changes in temperature cycles when applied to the layers towards increasing maximum temperature.

4. Conclusion

In the course of the work, a table of correspondence of the intensity value obtained from the infrared camera to the measured absolute temperature was developed. On the basis of the table, the data obtained from the IR camera were calibrated and thermal cycles were constructed. The temperature gradients in the horizontal direction of the layer and the vertical direction from the point of laser radiation exposure to the substrate were calculated. There is an increase in the maximum temperature and a corresponded decrease in the height of the layers. Shows the difference of the influence of population strategies on the temperature cycles and the temperature gradient. The observed results of temperature measurements correlate with defects on the wall surface and a deviation of geometry of the produced specimen. Presumably, the cause of defects was overheating of the sample, that is, the combined effect of factors of the high power of laser radiation and lack of model material.

Acknowledgements

The present study was carried out in frame of BAM internal project ProMoAm. The authors thank also Technische Universität Berlin for financial support of Mr. Stankevich as a part of the exchange program between TU Berlin and St. Petersburg Polytechnic University.

References

Vildanov AM, Babkin KD, Zemlyakov EV, Gushchina MO. The effects of beam oscillation on the quality of laser deposited metal parts. InJournal of Physics: Conference Series 2018 Nov (Vol. 1109, No. 1, p. 012059). IOP Publishing. DOI: 10.1088/1742-6596/1109/1/012059

Klimova-Korsmik O, Turichin G, Zemlyakov E, Babkin K, Petrovsky P, Travyanov A. Technology of High-speed Direct Laser Deposition from Ni-based Superalloys. Physics Procedia. 2016 Jan 1;83:716-22.DOI: 10.1016/j.phpro.2016.08.073

Turichin GA, Somonov VV, Babkin KD, Zemlyakov EV, Klimova OG. High-Speed Direct Laser Deposition: Technology, Equipment and Materials. Equipment and Materials. 2016 Apr;125(1):012009. DOI: 10.1088/1757-899X/125/1/012009

Turichin G, Zemlyakov E, Klimova O, Babkin K. Hydrodynamic instability in high-speed direct laser deposition for additive manufacturing. Physics Procedia. 2016 Jan 1;83:674-83.DOI: 10.1016/j.phpro.2016.09.001

Stankevich SL, Korsmik RS, Valdaytseva EA. Modeling of bead formation process during laser cladding. In Journal of Physics: Conference Series 2017 May (Vol. 857, No. 1, p. 012045). IOP Publishing. DOI: 10.1088/1742-6596/857/1/012045

Song, L., Bagavath-Singh, V., Dutta, B. and Mazumder, J., 2012. Control of melt pool temperature and deposition height during direct metal deposition process. The International Journal of Advanced Manufacturing Technology, 58(1-4), pp.247-256.

Peyre, P., Aubry, P., Fabbro, R., Neveu, R. and Longuet, A., 2008. Analytical and numerical modelling of the direct metal deposition laser process. Journal of Physics D: Applied Physics, 41(2), p.025403.

Han L, Liou FW, Phatak KM (2004) Modeling of laser cladding with powder injection. Metall Mater Trans B-Proc Metall Mater Proc Sci 35(6):1139–1150

Doubenskaia M, Bertrand P, Smurov I (2004) Optical monitoring of Nd: YAG laser cladding. Thin Solid Films 453:477–485. doi:10.1016/j.tsf.2003.11.184

Petrat T, Winterkorn R, Graf B, Gumenyuk A and Rethmeier M. (2018) Build-up strategies for temperature control using laser metal deposition for additive manufacturing Welding in the World 62, pp. 1073–1081

Everton, S.K., Hirsch, M., Stravroulakis, P., Leach, R.K. and Clare, A.T., 2016. Review of in-situ process monitoring and in-situ metrology for metal additive manufacturing. Materials & Design, 95, pp.431-445.